AIAA Paper 97-1505, Proceedings of the 14th Aerodynamic Decelerator Systems Technology Conference, San Francisco, California (1997).

AIAA-97-1505

# Parallel Computation of Parachute Fluid-Structure Interactions

Keith R. Stein* and Richard J. Benney†
U.S. Army Soldier Systems Command
Natick Research, Development and Engineering Center
Natick, MA 01760-5017

Vinay Kalro‡, Andrew A. Johnson§, and Tayfun E. Tezduyar¶
Aerospace Engineering and Mechanics
Army High Performance Computing Research Center
University of Minnesota
Minneapolis, MN 55415

## Abstract

The Army currently lacks the ability to predict accurately the behavior of parachute fluid-structure interaction phenomena. The interactions between the parachute system and the surrounding flow field are dominant in most parachute operations and thus the ability to predict parachute fluid-structure interaction phenomena is of interest to the Army.

This paper presents the current status of an ongoing research effort to couple the finite element formulations for the fluid dynamics and structural dynamics encountered in parachute problems. An application of the opening of an axisymmetric round parachute is presented. Future considerations for the coupled model and potential applications of interest to the Army are presented.

## Introduction

The dynamics of parachutes are complex and difficult to model accurately. During both the inflation process and the terminal descent stage, the dynamics of a parachute are governed by a highly nonlinear coupling between the structural dynamics of the parachute system and the surrounding fluid flow. Semiempirical parachute models require experimental data in order to adjust the model to represent parachute phenomena. However, these models break down if the simulated problem deviates from the problem the empirical data supports. In order to capture accurately time-variant parachute dynamics, the structural dynamics and fluid dynamics must be addressed as a coupled system[1].

Advances in high-performance computing (HPC) are making 3-D flow simulations and coupled fluid-structure computations for parachute problems more economical and feasible[2,3]. Finite element simulations for parachute problems require large, refined meshes, which result in large, nonlinear systems of equations. Parallel supercomputers and parallel implementation of solution algorithms are making these large-scale simulations much more realistic than in the past.

For the coupled parachute simulations, the time-dependent, 3-D Navier-Stokes equations governing the flow are solved using a stabilized space-time finite element formulation. In the space-time formulation, interpolation polynomials are functions of both space and time and the stabilized variational formulation of the problem is written over the space-time domain[4,5]. This formulation allows for the time-variation of the spatial domains to be automatically handled in the simulation. The problem is discretized with an unstructured finite element mesh to allow the arbitrary spatial domains encountered to be meshed efficiently. Finally, occasional remeshing of the spatial domain and projection of the solution from the previous mesh onto the new mesh allows for the solution of problems that experience large deformations.

The structural dynamics equations of motion are solved using a finite element formulation for a "tension structure" composed of cables and membranes. This formulation is being developed to be extended to a large class of parachutes, including round, gliding, and cross types parachutes[6,7].

This paper presents a method for the coupling of finite element formulations for the fluid dynamics and

---

* Aerospace Engineer
† Aerospace Engineer, Member AIAA
‡ Research Associate
§ Research Assistant Professor
¶ Professor

structural dynamics encountered in parachute problems. An application of the opening of an axisymmetric round parachute is presented. Finally, future considerations for the coupled model and potential applications of interest to the Army are presented.

## Theory

(1) Computational Fluid Dynamics (CFD) Model-

Navier-Stokes Equations-

Let $\Omega_t \subset \Re^{nsd}$ and (0,T) be the spatial and temporal domains, respectively, where nsd is the number of space dimensions, and let $\Gamma_t$ denote the boundary of $\Omega_t$. The subscript "t" implies the time-dependence of the spatial domain. The spatial and temporal coordinates are denoted by $\mathbf{x}=(x,y,z)$ and $t \in (0,T)$. The Navier-Stokes equations for incompressible flows are

$$\begin{aligned} \rho\left(\frac{\partial \boldsymbol{u}}{\partial t}+\boldsymbol{u}\cdot\nabla\boldsymbol{u}+\boldsymbol{f}\right)-\nabla\cdot\sigma=0 \qquad & on\ \ \Omega_t, \\ \nabla\cdot\boldsymbol{u}=0 \qquad & on\ \ \Omega_t, \end{aligned} \tag{1}$$

where $\rho$ is constant density and $\mathbf{u}=(u,v,w)$ is the velocity vector. Here $\mathbf{f}$ is an external force term consisting of gravity. For the Newtonian fluids under consideration, the stress tensor for a fluid with dynamic viscosity $\mu$ is defined as follows:

$$\begin{aligned} \sigma(p,\boldsymbol{u}) &= -pI+2\mu\epsilon(\boldsymbol{u}) \\ \epsilon(\boldsymbol{u}) &= \frac{1}{2}\left(\nabla\boldsymbol{u}+(\nabla\boldsymbol{u})^T\right). \end{aligned} \tag{2}$$

Both the Dirichlet and Neumann-type boundary conditions are accounted for, as represented by

$$\begin{aligned} \boldsymbol{u} &= \boldsymbol{g} \qquad on\ \ (\Gamma_t)_g, \\ \boldsymbol{n}\cdot\sigma &= \boldsymbol{h} \qquad on\ \ (\Gamma_t)_h, \end{aligned} \tag{3}$$

where $(\Gamma_t)_g$ and $(\Gamma_t)_h$ are complementary subsets of the boundary $\Gamma_t$. The initial condition on the velocity is specified as $\mathbf{u}(x,0)=\mathbf{u}_0$ on $\Omega_0$, where $\mathbf{u}_0$ is divergence free.

Deformable-Spatial-Domain/Stabilized-Space-Time (DSD/SST) Formulation-

In order to construct the finite element function spaces for the space-time method, we partition the time interval (0,T) into subintervals $I_n=(t_n,t_{n+1})$, where $t_n$ and $t_{n-1}$ belong to an ordered series of time levels $0=t_0<t_1<\ldots<t_N=T$. Let $\Omega_n=\Omega_{t_n}$ and $\Gamma_n=\Gamma_{t_n}$. We define the space-time slab $Q_n$ as the domain enclosed by the surfaces $\Omega_n$, $\Omega_{n+1}$, and $P_n$, where $P_n$ is the surface described by the boundary $\Gamma_t$ as t traverses $I_n$. As is the case with $\Gamma_t$, surface $P_n$ is decomposed into $(P_n)_g$ and $(P_n)_h$ with respect to the type of boundary condition (Dirichlet or Neumann) being imposed. For each space-time slab we define the corresponding finite element function spaces $(S_u^h)_n$, $(V_u^h)_n$, $(S_p^h)_n$, and $(V_p^h)_n$. Over the element domain, this space is formed by using first-order polynomials in space and time. Globally, the interpolation functions are continuous in space but discontinuous in time.

The stabilized space-time formulation for deforming domains is then written as follows: given $(\mathbf{u}^h)_n^-$, find $\mathbf{u}^h \in (S_u^h)_n$ and $p^h \in (S_p^h)_n$ such that $\forall\ \mathbf{w}^h \in (V_u^h)_n$ and $q^h \in (V_p^h)_n$

$$\begin{aligned} &\int_{Q_n} \boldsymbol{w}^h\cdot\rho\left(\frac{\partial \boldsymbol{u}^h}{\partial t}+\boldsymbol{u}^h\cdot\nabla\boldsymbol{u}^h+\boldsymbol{f}^h\right)dQ \ + \int_{Q_n}\nabla\boldsymbol{w}^h:\sigma(p^h,\boldsymbol{u}^h)dQ \\ &+\int_{Q_n} q^h\nabla\cdot\boldsymbol{u}^h dQ \ + \int_{\Omega_n}(\boldsymbol{w}^h)_n^+\cdot\rho\left((\boldsymbol{u}^h)_n^+-(\boldsymbol{u}^h)_n^-\right)d\Omega \\ &+\sum_{e=1}^{n_{el}}\int_{Q_n^e}\frac{\tau}{\rho}\left[\rho\left(\frac{\partial \boldsymbol{w}^h}{\partial t}+\boldsymbol{u}^h\cdot\nabla\boldsymbol{w}^h\right)-\nabla\cdot\sigma(q^h,\boldsymbol{w}^h)\right]\cdot \\ &\left[\rho\left(\frac{\partial \boldsymbol{u}^h}{\partial t}+\boldsymbol{u}^h\cdot\nabla\boldsymbol{u}^h+\boldsymbol{f}^h\right)-\nabla\cdot\sigma(p^h,\boldsymbol{u}^h)\right]dQ \ + \\ &\sum_{e=1}^{n_{el}}\int_{Q_n^e}\delta\nabla\cdot\boldsymbol{w}^h\rho\nabla\cdot\boldsymbol{u}^h dQ \ = \int_{(P_n)_h}\boldsymbol{w}^h\cdot\boldsymbol{h}^h dP \end{aligned} \tag{4}$$

This process is applied sequentially to all the space-time slabs $Q_1$, $Q_2$, ..., $Q_{N-1}$. In equation 4, the following notation is used:

$$\begin{aligned} (\boldsymbol{u}^h)_n^{\pm} &= \lim_{\epsilon\to 0}\boldsymbol{u}(t_n\pm\epsilon), \\ \int_{Q_n}(\ldots)dQ &= \int_{I_n}\int_{\Omega_t}(\ldots)d\Omega\,dt \end{aligned} \tag{5}$$

The computations start with $(\mathbf{u}^h)_0^- = \mathbf{u}_0$.

In the variational formulation given by equation 4, the first four terms and the right-hand-side constitute the Galerkin formulation of the problem. The first series of element-level integrals are least-squares terms based on the momentum equation. The second series of element-level integrals are added to the formulation for numerical stability at high Reynolds numbers. These are least-squares terms based on the continuity equation.

The stabilization coefficients $\tau$ and $\delta$ are defined at the element level. Both stabilization terms are weighted residuals, and therefore maintain the consistency of the formulation. Since the interpolation functions are discontinuous in time, the fourth term weakly enforces continuity of the velocity field across the space-time slabs.

Axisymmetric Assumption-

For the axisymmetric equations, the stress terms and continuity equation take a different form than for the 2-D Cartesian equations. For axisymmetry, we use cylindrical coordinates with $u_\theta=0$, $\partial u/\partial\theta=0$, and $\partial v/\partial\theta=0$. The x-axis will be the symmetry axis and the y-axis will be the radial axis.

Solution Method-

Each time step, the resulting nonlinear system of equations from the DSD/SST formulation are solved using a Newton-Raphson iterative method. At each nonlinear iteration a linear system of equations is solved iteratively with the GMRES update technique[8]. Use of an iterative solver substantially reduces the cost compared to direct solvers and also eliminates the need to store the global matrix. Following each nonlinear iteration, the nodal positions for the finite element mesh at time $n+1$ are updated to account for the motions of the boundary representing the parachute surface. The update of the mesh nodes is accomplished using an automatic mesh moving scheme, which treats the nodes as material points on a linear elastic solid[9]. This linear elastic solid has no significance to the physical problem but offers a method for handling the mesh deformations. The approach is able to handle arbitrary deformations of the mesh boundaries but introduces an extra cost into the computation with the formulation and solution of an additional set of equations for the linear elastic solid. At the end of each time step, the mesh quality (i.e., distortion) is checked. If the mesh fails prescribed quality checks, a remesh is performed; the solution is projected onto the new mesh, and the solution continues with the new mesh for the next time step.

(2) Structural Dynamic (SD) Model-

Approach-

The parachute structure is modeled as a system of axisymmetric membrane elements for the canopy, cable elements for the suspension lines, and a concentrated mass "element" for the payload. The equations of motion for the structural model are developed from the principle of virtual work shown below[6]:

$$0=\int\int({}'n^{\alpha\beta}\ \delta\gamma_{\alpha\beta}-{}'p_i\ \delta u_i)\ \sqrt{A}dx_1dx_2+ h\int\int\rho\ {}'\ddot{u}_i\delta u_i\sqrt{A}dx_1dx_2 \qquad (6)$$

where $\delta\gamma_{\alpha\beta}$ is the infinitesimal virtual strain corresponding to a small virtual displacement $\delta u_i$ superposed on the nonlinear displacement $u_i$ to the deformed configuration $'C$. The coordinates $x_i$ correspond to the original configuration $^oC$. $A$ is the determinant of the metric tensor of $^oC$ and $n^{\alpha\beta}$ are the membrane stress resultants on $'C$. The force vector $\boldsymbol{F}$ is given by

$$\boldsymbol{F}\sqrt{{}'A}dx_1dx_2={}'p_i\sqrt{A}dx_1dx_2\hat{e}_i \qquad (7)$$

and has been expressed in terms of Cartesian components ${}'p_i$. $\rho$ is the density in $^oC$, ${}'\ddot{u}_i$ is the acceleration of $'C$, $'A$ is the determinant of the metric tensor of $'C$, and $\hat{e}_i$ are the Cartesian base vectors .

In addition to the internal forces, conservative gravitational forces are imposed on each element type, and nonconservative time-dependent pressure induced forces are imposed on the membrane elements. For the axisymmetric problem, the only constraints imposed are that the concentrated mass (payload) element is required to remain on the symmetry axis ($r=0$) and the vent node for the axisymmetric membrane (canopy) elements has a fixed radius ($r=r_v$). Thus, the structural model is free to fall under the net influence of gravity and the imposed pressure distribution.

For the axisymmetric representation of a round parachute, no curvature in individual gores can be represented in the circumferential direction. Positive hoop forces (i.e., in tension) can only be experienced at a membrane material point when the radius of the material for the deformed geometry from the symmetry axis exceeds the undeformed radius (i.e., constructed radius) for the material point. For the problem presented, positive hoop forces are experienced only in the near vicinity of the vent of the axisymmetric parachute model. To account for a membrane that cannot exhibit compressive forces, wrinkling is approximated by "turning off" the hoop contributions for the regions of the membrane that are in compression.

Solution Method-

The Newmark Method is used to solve dynamic simulations within the SD code. The resulting nonlinear system of equations from the SD formulation is solved

using a Newton-Raphson iterative method. At each nonlinear iteration the linear system of equations is solved directly with a skyline method[6].

(3) Coupling-

For the coupled simulation, the SD code is embedded in the nonlinear iteration loop of the CFD code. The CFD and SD models are coupled along a set of nodes defining the parachute surface. By prescribing parachute membrane nodes in the SD model that are identical to the parachute boundary nodes in the CFD mesh, we eliminate any need for interpolation as information is passed between the two codes. For the coupled solution, multiple SD time steps are solved for each CFD time step, and the CFD time step is equivalent to the time step of the coupled simulation.

The strategy used to couple the CFD and SD codes is shown in Figure 1. Within the time step loop for the coupled simulation is a nonlinear iteration loop, which involves three primary tasks each iteration. First, the SD solution is advanced one coupled time step (i.e., multiple SD time steps) using the most updated pressure distribution from the CFD solution. Since multiple SD time steps occur over one CFD space-time slab, a ramped pressure distribution is fed as input to the SD code. This pressure ramp is interpolated from the linear nodal pressures from the DSD/SST solution. It should be noted that substepping in time of the SD solution requires a subiteration to solve the nonlinear SD equations each SD time step. Prescribing equal time steps for the CFD and SD codes would eliminate the requirement to subiterate for the SD solution. Second, the CFD mesh for the advanced time, $n+1$, is moved to fit the updated nodal positions as computed from the SD code in step 1. Third, the CFD system of equations is iterated on using the updated mesh and imposing the updated velocities from the SD solution as boundary conditions.

The coupled code is implemented on the CM-5 parallel supercomputer. The equation system for the SD solution is very small relative to the CFD equation system. For this reason, the SD portion of the coupled code is not currently programmed to utilize the strengths of parallel computers, but instead runs on the front-end of the CM-5. In contrast, the CFD portion of the code is programmed for the CM-5 and substantial speedups are experienced mainly in the parallel formulation of the CFD system of equations and the parallel solution of the linear system with the GMRES iterative method.

An underrelaxation approach is used throughout the iterative process in order to permit the solution to converge. This was necessary due to the sensitivity of the membrane to predicted pressure loadings. Thus, for iteration $I+1$, the pressure sent to the SD code is $p=(1-\alpha)p_i+\alpha p_{i+1}$, where $\alpha$ is the underrelaxation coefficient and was given a value of 0.1. Underrelaxation has a drawback in that it forces the coupled solution to converge less efficiently.

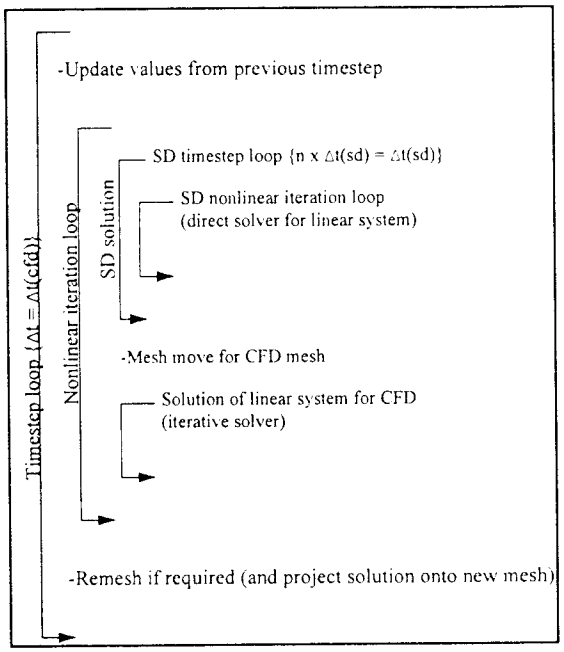


**Figure 1**: Coupling Algorithm

Finally, for the coupled simulation, the hoop contribution in the SD model introduced noise as nodes near the apex transitioned from states of positive hoop stress to "wrinkled." For this reason, the hoop term was turned off for all nodes in the presented simulation. In order to account for the hoop contribution, the SD model may need to smoothly transition nodes from "hoop stressed" to "hoop wrinkled" states.

## Sample Problem

For the following simulation, a round parachute was represented by a system composed of 70 axisymmetric membrane elements, 10 cable elements, and one concentrated mass element. The initial condition for the problem is that the canopy-suspension line-concentrated mass system is suspended at rest in its nonstressed configuration. At the start of the simulation, gravity is "turned on" to initiate the motion of the parachute system. The axisymmetric membrane elements modeled a flat circular parachute construction

of nondimensional radius 1.25 with a vent radius of 0.075. The membrane elements were given thickness of 0.003. The membrane material properties had a density of 12.0 and a Young's modulus of 12,000. The Poisson effect in the membrane was not accounted for since the hoop terms were turned off. The cable elements represented suspension lines of length 1.64 times the constructed radius of the membrane. The cables were defined to model the net effect of 28 suspension lines. This was accomplished by defining a cable area of 28 times the area of one cable. The cross-sectional area for the cable elements was 0.001. The cable material properties had a density of 12.0 and a Young's modulus of 12,000. The concentrated mass was given a mass of 0.5. Each of the element types fell under the influence of gravity, with a gravitation constant of -2.5 in the vertical direction. It should be noted that the SD model is not utilizing any damping options for this simulation and any damping effects are a result of natural fluid-structure damping.

The fluid dynamics model used an unstructured triangular mesh in which each parachute surface node was represented by two nodes; one node for the outer parachute surface, and one node for the inner surface. The number of elements in the mesh varied due to the occasional remeshing of the CFD domain, but the mesh size typically ranged from 5000-8000 elements. For the sample problem, the Reynolds number based on the projected radius varied in time and had a maximum value of about 7500.

The simulation for the sample problem was run until a "steady-state" solution was approached. Due to the stretchiness of the cables (i.e., suspension lines), the solution was still oscillating significantly at the end of the simulation. Shown in Figure 2 are the time histories for the predicted vertical positions of the apex node, skirt node, and payload node. Figures 3 and 4 show the computed geometries of the structural model at equally spaced instances in time displayed on top of the payload vertical position time history. These plots show the inflation sequence as the canopy inflates, overinflates and collapses due to wake recontact and approaches a fully inflated "steady-state" geometry. It should be noted that the stretchiness of the cables is largely responsible for the severity of the shown collapse. The properties prescribed to the cables result in a "bungee effect" that actually causes the concentrated mass element (i.e., payload) to rebound upward for a brief period following the initial inflation, which is evident in Figure 2.

Predicted velocities for the apex node, skirt node, and payload node are shown in Figure 5. The

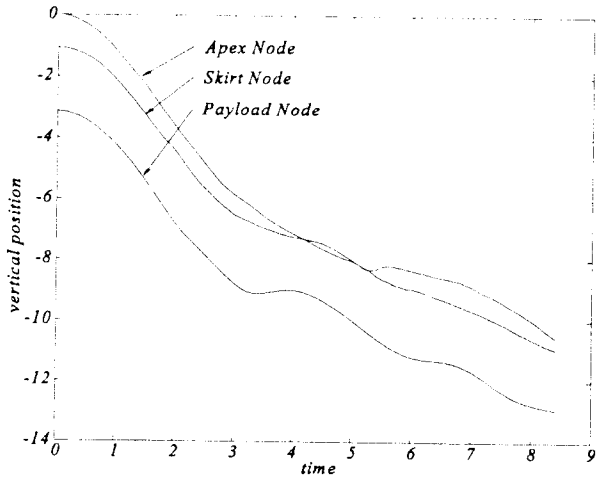


**Figure 2**: Vertical Position Time Histories

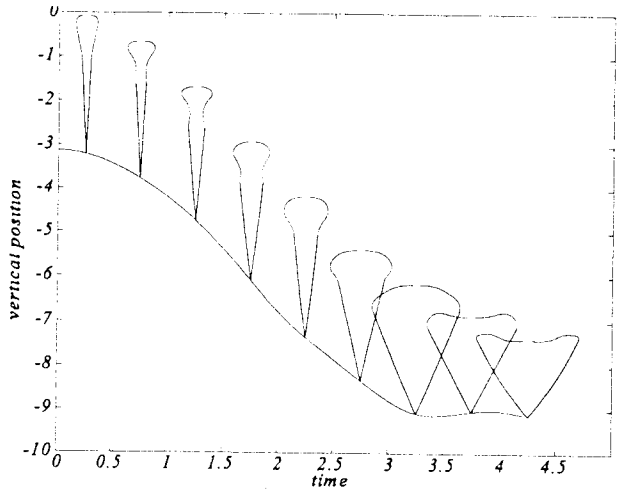


**Figure 3**: Computed Geometries

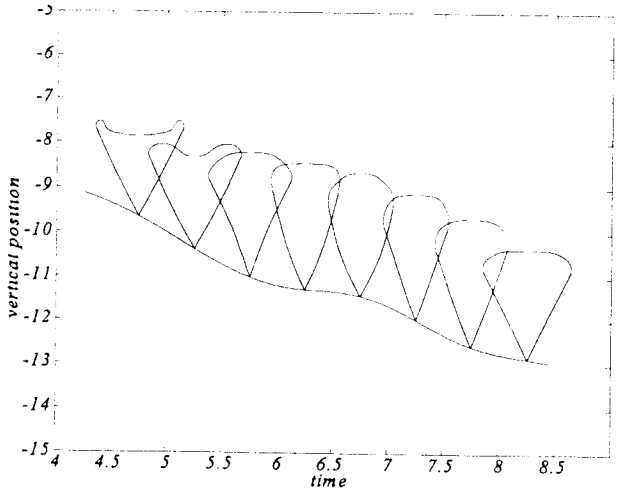


**Figure 4**: Computed Geometries

relationship between the time histories of the three nodes shows the relative positions and motions for the deforming structural systems throughout the inflation process. The spike in the curve for the apex nodes corresponds to the short time period during which the canopy transitions from its collapsed configuration and begins to reinflate. The high frequencies experienced during the later times are largely due to the vibrations in the cables, which have no damping. Future simulations will incorporate approximations for line drag in the SD model, which are expected to naturally damp a great deal of these oscillations[7].

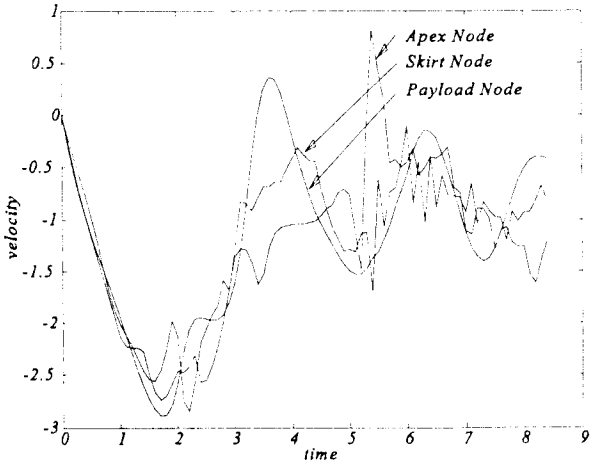


**Figure 5**: Vertical Velocity Time Histories

Figure 6 shows the projected area and skirt area for the axisymmetric parachute throughout the inflation process. For this simulation, it is evident that during the overinflation and collapse of the canopy, the skirt radius approaches the maximum radius on the canopy.

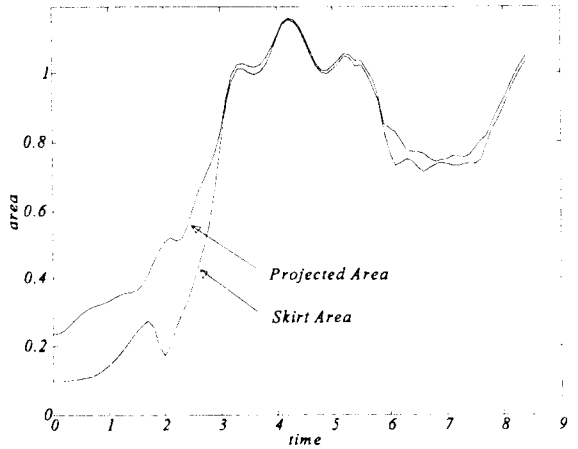


**Figure 6**: Project and Skirt Area Time Histories

Figure 7 shows the histories of various forces throughout the simulation. The payload node experiences a gravitational force due to the mass of the concentrated mass element and one half of the mass of the adjacent cable element. The payload node also experiences a force due to the tension in the adjacent cable element. In steady state, the gravitational force should balance the vertical component of the tensile force, since for the presented problem there are no other forces acting on the payload. The figure shows that the net force on the payload is oscillating and slowly damping about 0.0. The frequency of these oscillations is low, primarily due to the unrealistically low stiffness in the cable elements. Also shown is the time history of the aerodynamic force on the canopy. This pressure force is integrated from the predicted time-variant pressure distribution. It should be noted that the higher frequency oscillations towards the end of the simulation are largely due to the undamped vibrations in the cables. Also, some noise is periodically introduced into the pressures when the CFD mesh is remeshed.

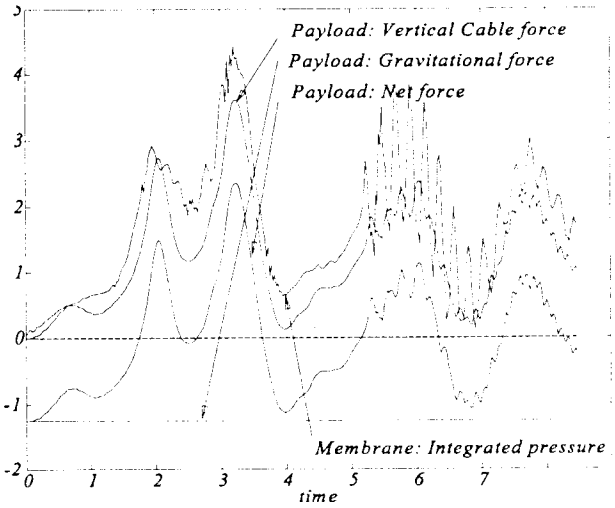


**Figure 7**: Force Time Histories

Figure 8 shows the predicted flow fields at equally spaced instances in time during the time period surrounding the canopy overinflation. The right side of the figures shows the contours of constant pressure with the arrows indicating the directions of increasing pressure from the p=0.0 contour. The pressure difference between contours is 0.25. The left side of the figures shows the velocity vector fields relative to the motion of the apex node.

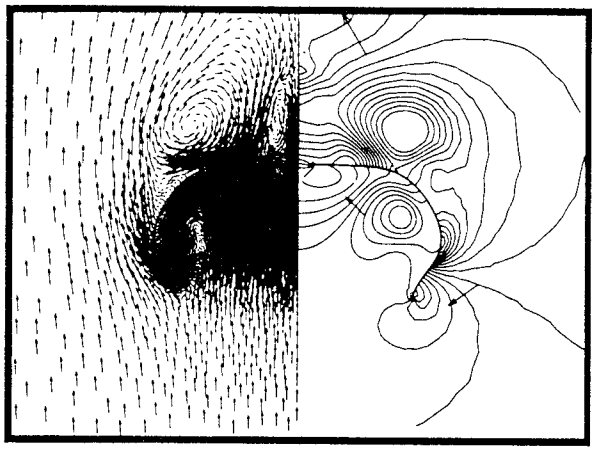

time=2.85

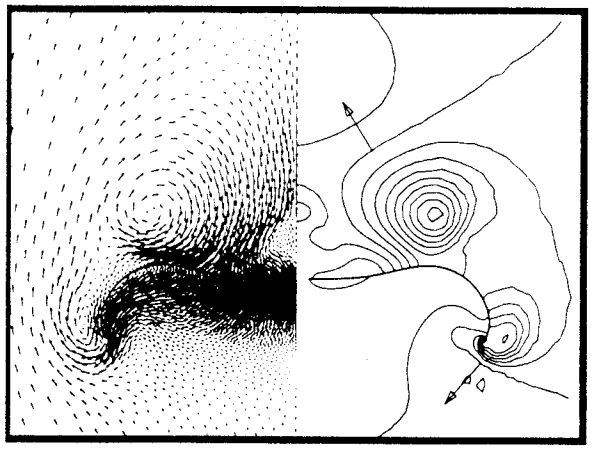

time=3.65

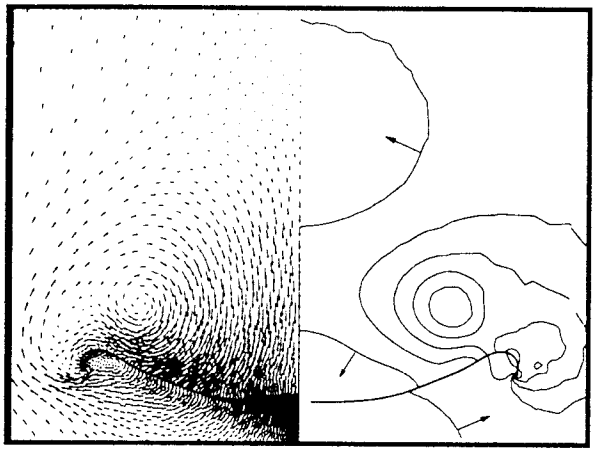

time=4.45

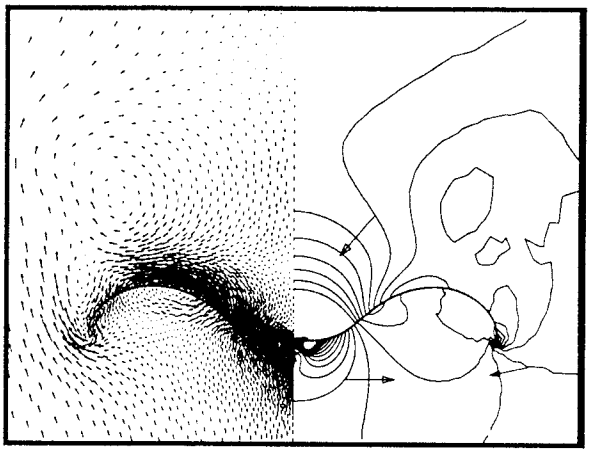

time=5.25

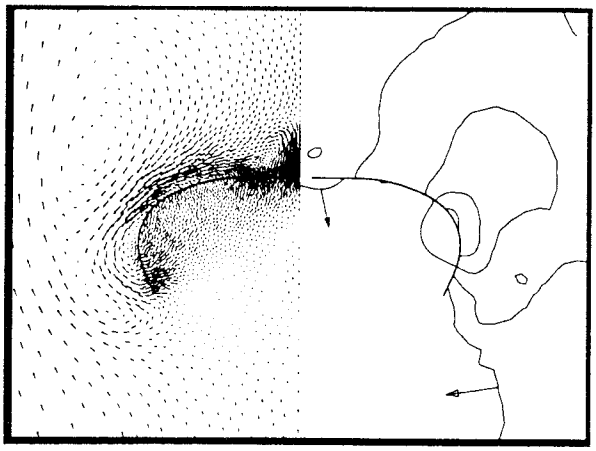

time=6.05

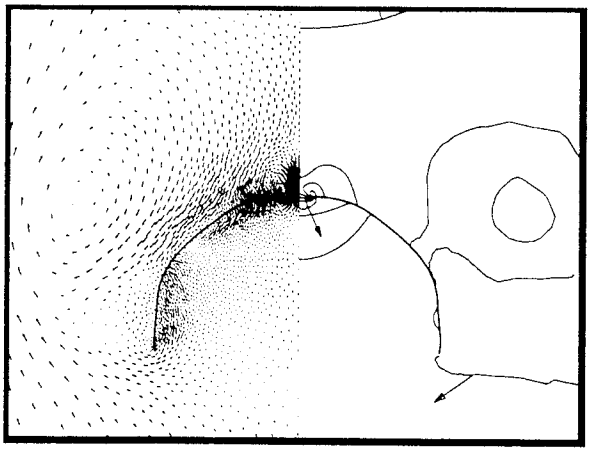

time=6.85

**Figure 8:** Predicted Velocity and Pressure Flowfields at Various Times

## Conclusions

We have presented the current status of an ongoing research effort to model fluid-structure interaction phenomena experienced by parachute systems. These codes are more tightly coupled than previous models, which were coupled explicitly in time. They are able to handle much more arbitrary deformation than previous models could handle due to the use of unstructured meshes, an automatic mesh moving scheme, and through occasional remeshing of the CFD mesh. These capabilities allow for representation of initial geometries that are closer to line stretch configurations, the ability to represent vents, and more overall flexibility than with previous models. In addition, the CFD portions of the code have been parallelized to take advantage of the strengths of todays high-performance computers. The SD portions of the code are currently being parallelized.

Some potential enhancements to the current model have been alluded to and will include utilizing the line drag built into the SD code, addressing problems with nonzero initial velocity deployments, improvement of convergence during the numerical simulation, and better representation of the hoop term in the SD model. Coupling of the axisymmetric flow with the 3-D representation of a single gore along the meridian set of SD nodes would improve the hoop representation for the model.

Although the presented problem was for an axisymmetric representation of a parachute, the coupling approach for 3-D problems will take a parallel approach. Both the SD and CFD capabilities have been demonstrated and are ready for coupling in 3-D. Initial simulations have focused on axisymmetric simulation due to the reduced computational size for this problem. However, future 3-D coupling will allow for a much broader range of problems to be addressed. A few of the 3-D fluid-structure interaction problems that would be of great interest to the Army include the opening of round parachutes, ram-air performance, response of parachutes to cross-wind/gusts, initial deployment characteristics. With a fully-coupled 3-D capability, these problems, which previously could be addressed only by experimental approaches or semiempirically, will benefit from the advantages of numerical simulations.

## Acknowledgment

This research was supported in part by NASA-Johnson Space Center (grant number NASA/NAG9-919), by ARO (grant number DAAH04-93-G-0514), and the Army High Performance Computing Research Center under the auspices of the Department of the Army, Army Research Laboratory cooperative agreement number DAAH04-95-2-0003/contract number DAAH04-95-0008. CRAY time was provided in part by the University of Minnesota Supercomputer Institute.

## References

1. R.J. Benney and K.R. Stein. "A Computational Fluid Structure Interaction Model For Parachute Inflation." *Journal of Aircraft*, **33** (1996) 730-736.

2. V. Kalro, S. Aliabadi, W. Garrard, T. Tezduyar, and K. Stein. "Parallel Finite Element Simulation of Large Ram-Air Parachutes." *International Journal for Numerical Methods in Fluids*, ~~in press.~~ **24** (1997) 1353-1369.

3. S.K. Aliabadi, W.L. Garrard, V. Kalro, S. Mittal, T.E. Tezduyar, and K.R. Stein. "Parallel Finite Element Computation of the Dynamics of Large Ram Air Parachutes." *13th Aerodynamic Decelerator Technology Conference*. Paper AIAA-95-1581-CP. Clearwater, FL, 1995.

4. T.E. Tezduyar, M. Behr, and J. Liou. "A New Strategy for Finite Element Computations Involving Moving Boundaries and Interfaces -- the Deforming-Spatial-Domain/Space-Time Procedure: I. The Concept and the Preliminary Tests." *Computer Methods in Applied Mechanics and Engineering*, **94** (1992) 339-351.

5. T.E. Tezduyar, M. Behr, S. Mittal, and J. Liou. "A New Strategy for Finite Element Computations Involving Moving Boundaries and Interfaces -- the Deforming-Spatial-Domain/Space-Time Procedure: II. Computation of Free-surface Flows, Two-liquid Flows, and Flows with Drifting Cylinders." *Computer Methods in Applied Mechanics and Engineering*, **94** (1992) 353-371.

6. R.J. Benney and J.W. Leonard. "A 3-D Finite Element Structural Parachute Model." *13th Aerodynamic Decelerator Technology Conference*. Paper AIAA-95-1563-CP. Clearwater, FL, 1995.

7. R.J. Benney, K.R. Stein, J.W. Leonard, and M.L. Accorsi. "Current 3-D Finite Element Modeling Capabilities." *14th Aerodynamic Decelerator Technology Conference*. San Francisco, CA, 1997.

8. Y. Saad and M. Schultz. "GMRES: A Generalized Minimal Residual Algorithm for Solving Nonsymmetric Linear Systems." *SIAM Journal of Scientific and Statistical Computing*, 7 (1986) 856-869.

9. A.A. Johnson and T.E. Tezduyar. "Mesh Update Strategies in Parallel Finite Element Computations of Flow Problems with Moving Boundaries and Interfaces." *Computer Methods in Applied Mechanics and Engineering*, **119** (1994) 73-94.